Magn Reson Med Sci 2020; 19; 99–107
doi:10.2463/mrms.mp.2019-0030 Published Online: May 7, 2019

MAJOR PAPER

Utility of Stack-of-stars Acquisition for Hepatobiliary Phase Imaging without Breath-holding

Shintaro Ichikawa[1], Utaroh Motosugi[1*], Marie-Luise Kromrey[1], Daiki Tamada[1], Tetsuya Wakayama[2], Kang Wang[3], Ty A Cashen[3], Ali Ersoz[4], and Hiroshi Onishi[1]

Purpose: Post-contrast liver magnetic resonance imaging is typically performed with breath-hold 3D gradient echo sequences. However, breath-holding for >10 s is difficult for some patients. In this study, we compared the quality of hepatobiliary phase (HBP) imaging without breath-holding using the prototype pulse sequences stack-of-stars liver acquisition with volume acceleration (LAVA) (LAVA Star) with or without navigator echoes (LAVA $Star_{navi+}$ and LAVA $Star_{navi-}$) and Cartesian LAVA with navigator echoes (Cartesian $LAVA_{navi+}$).

Methods: Seventy-two patients were included in this single-center, retrospective, cross-sectional study. HBP imaging using the three LAVA sequences (Cartesian $LAVA_{navi+}$, LAVA $Star_{navi-}$, and LAVA $Star_{navi+}$) without breath-holding was performed for all patients using a 3T magnetic resonance system. Two independent radiologists qualitatively analyzed (overall image quality, liver edge sharpness, hepatic vein clarity, streak artifacts, and respiratory motion/pulsation artifacts) HBP images taken by the three sequences using a five-point scale. Quantitative evaluations were also performed by calculating the liver-to-spleen, -lesion, and -portal vein (PV) signal intensity ratios. The results were compared between the three sequences using the Friedman test.

Results: LAVA $Star_{navi+}$ showed the best image quality and hepatic vein clarity ($P < 0.0001$). LAVA $Star_{navi-}$ showed the lowest image quality ($P < 0.0001$–0.0106). LAVA $Star_{navi+}$ images showed fewer streak artifacts than LAVA $Star_{navi-}$ images ($P < 0.0001$), while Cartesian $LAVA_{navi+}$ images showed no streak artifacts. Cartesian $LAVA_{navi+}$ images showed stronger respiratory motion/pulsation artifacts than the others ($P < 0.0001$). LAVA $Star_{navi-}$ images showed the highest liver-to-spleen ratios ($P < 0.0001$–0.0005). Cartesian $LAVA_{navi+}$ images showed the lowest liver-to-lesion and -PV ratios ($P < 0.0001$–0.0108).

Conclusion: In terms of image quality, the combination of stack-of-stars acquisition and navigator echoes is the best for HBP imaging without breath-holding.

Keywords: *breath-hold, gadoxetic acid, hepatobiliary phase, respiratory navigation, stack-of-stars*

Introduction

Gadoxetic acid is a liver-specific contrast agent that is widely used in liver MRI. It is taken up by hepatocytes via the membrane transporter,[1] yielding hepatobiliary phase (HBP) images with excellent liver enhancement and liver-to-lesion contrast 15–20 min after the contrast injection. Previous reports have shown that HBP images are helpful in increasing the diagnostic accuracy and sensitivity for hepatocellular carcinoma (HCC) or liver metastases.[2–4] High-quality HBP images are essential for favorable diagnostic performance on gadoxetic acid-enhanced MRI. Cartesian *k*-space sampling with the breath-hold technique has been widely used for HBP imaging. However, conventional techniques require approximately 15–20 s of breath-holding. The high-risk group in HCC mainly consists of elderly patients and often shows complications such as respiratory dysfunction or hearing loss. In such patients, image quality may be impaired with respiratory motion artifacts on breath-hold acquisition,

[1]Department of Radiology, University of Yamanashi, 1110 Shimokato, Chuo-shi, Yamanashi 409-3898, Japan
[2]MR Collaboration and Development, GE Healthcare, Tokyo, Japan
[3]MR Collaboration and Development, GE Healthcare, Madison, WI, USA
[4]MR Engineering, GE Healthcare, Waukesha, WI, USA
[*]Corresponding author, Phone: +81-55-273-1111, Fax: +81-55-273-6744, E-mail: umotosugi@nifty.com

©2019 Japanese Society for Magnetic Resonance in Medicine
This work is licensed under a Creative Commons Attribution-NonCommercial-NoDerivatives International License.

Received: December 22, 2018 | Accepted: March 17, 2019

leading to diagnostic inaccuracy. A respiratory-triggered 3D T_1-weighted technique has been proposed as an alternative to the breath-hold technique.[5,6] Recently, a radial sampling technique including stack-of-stars acquisition has been used as a *k*-space sampling trajectory for fast MRI to achieve more motion robustness.[7–9] Conventional Cartesian acquisition involves rectilinear sampling, whereas stack-of-stars acquisition uses Cartesian sampling along the *z*-axis and radial sampling along the *xy*-plane (Fig. 1). This technique offers several advantages over Cartesian sampling, including diminished motion artifacts due to the continuous update of the *k*-space center[10] and its suitability for high under-sampling factors.[7]

The major disadvantages of radial sampling are the streak artifacts resulting from under-sampling,[7] decreased signal-to-noise ratio,[11] and more complex image reconstruction. Stack-of-stars acquisition has been used in many MRI applications, including gadoxetic acid-enhanced MRI.[12–14]; however, few studies have attempted to identify the best type of protocol for HBP imaging without breath-holding in clinical practice. We hypothesized that the combination of stack-of-stars acquisition and respiratory navigation may improve the image quality of HBP imaging without breath-holding. Thus, the aim of this study was to compare the quality of HBP imaging using the prototype pulse sequences stack-of-stars liver acquisition with volume acceleration (LAVA) (LAVA Star) with or without navigator echoes (LAVA $Star_{navi+}$ and LAVA $Star_{navi–}$) and Cartesian LAVA with navigator echoes (Cartesian $LAVA_{navi+}$).

Materials and Methods

Patients

This single-center, retrospective, cross-sectional study was performed in accordance with the principles outlined in the Declaration of Helsinki and was approved by the relevant Institutional Review Board. The requirement for written informed consent was waived due to the retrospective nature of the study. Seventy-two consecutive patients (39 men and 33 women; mean age, 68.0 ± 12.7 [range, 22–90] years; mean body weight, 58.3 ± 10.8 [range, 39–88] kg) who underwent gadoxetic acid-enhanced MRI between May and June 2018 were included in this study. Fifty-three patients (73.6%) had chronic liver disease with the following causes: hepatitis C (n = 30), hepatitis B (n = 13), alcoholic steatohepatitis (n = 4), nonalcoholic steatohepatitis (n = 2), autoimmune hepatitis (n = 1), idiopathic portal hypertension (n = 1), and unidentified liver disease with an elevated liver enzyme level (n = 2). Thirty HCCs (10 early HCCs and 20 hypervascular HCCs; mean size, 10.3 ± 6.6 [range, 5–35] mm) were observed in 18 patients. Diagnoses were performed on the basis of pathological evaluation in two cases and imaging findings in 28 cases.

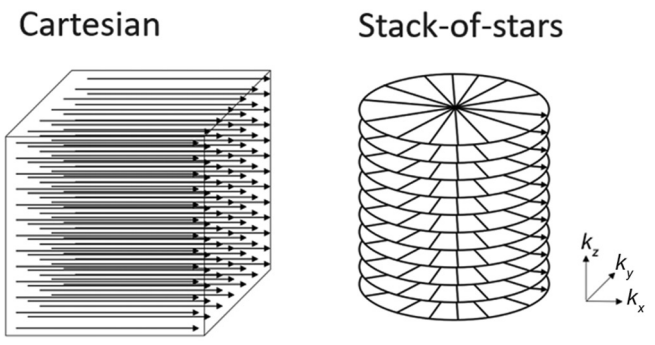

Fig. 1 Schema of Cartesian and stack-of-stars acquisition. Conventional Cartesian acquisition involves rectilinear sampling (**left**), whereas the stack-of-stars technique uses Cartesian sampling along the *z*-axis and radial sampling along the *xy*-plane (**right**).

Hepatobiliary phase imaging

Gadoxetic acid-enhanced MRI was performed using a 3T MR system (Discovery 750; GE Healthcare, Waukesha, WI, USA) with a 32-channel phased-array coil. Gadoxetic acid (0.025 mmol/kg body weight) was administered at a rate of 1 mL/s followed by a 20-mL saline flush by using a power injector. About 15 min after injection of gadoxetic acid, four different LAVA acquisitions were performed in the following order: Cartesian $LAVA_{navi+}$, LAVA $Star_{navi+}$, Cartesian breath-hold LAVA, and LAVA $Star_{navi–}$. The three LAVA sequences (Cartesian $LAVA_{navi+}$, LAVA $Star_{navi–}$, and LAVA $Star_{navi+}$) without breath-holding were used for evaluation in this study. Sequence parameters are summarized in Table 1. The acquisition times of those three sequences are as follows: Cartesian $LAVA_{navi+}$, ~3 min; LAVA $Star_{navi–}$, 1 min; and LAVA $Star_{navi+}$, ~5 min.

Stack-of-stars acquisition (LAVA Star) and navigator echoes

The gradient echo with stack-of-stars sampling was developed as shown in Fig. 1. A golden angle scheme was used for in-plane radial sampling.[7,13] In each radial angle, the necessary Cartesian data in the k_z direction were successively collected before moving to the next radial angle. A spectrally selective inversion pulse was applied intermittently for fat suppression in each radial angle. For LAVA $Star_{navi+}$ acquisition, pencil beam excitation was used for navigator gating. The acquired radial sampling *k*-space data were gridded, after which Fourier transformation was applied to the gridded Cartesian *k*-space data followed by gridding kernel correction.[15,16]

Image interpretation

Two independent radiologists (S.I. and M.L.K., with 11 and 3 years of clinical experience in abdominal MRI, respectively) who were blinded to the clinical data performed qualitative and quantitative analyses of HBP imaging. For each dataset, the following parameters of image quality and artifacts were assessed using a five-point visual score, with the highest score indicating the most desirable examination for parameters

Table 1 Sequence parameters of breath-hold-free hepatobiliary phase imaging

	Cartesian LAVA with navigator echoes	LAVA Star without navigator echoes	LAVA Star with navigator echoes
Plane	Transverse	Transverse	Transverse
Slice thickness/spacing between slices (mm)	3.6/1.8	3.6/1.8	3.6/1.8
Flip angle (°)	25	25	25
Repetition time/echo time (ms)	4.48/1.71	4.55/1.69	4.55/1.69
Band width (Hz/px)	488.3	488.3	488.3
Parallel imaging factor (ARC) (phase/slice)	2.0/1.5	-	-
Matrix (read × phase or spokes)	320 × 224	320 × 224	320 × 224
Field of view (cm)	34	36	36
Number of signal averaged	0.7	0.7	0.7

LAVA, liver acquisition with volume acceleration; ARC, auto-calibrating reconstruction for Cartesian sampling.

of image quality and artifacts; overall image quality, liver edge sharpness, hepatic vein clarity, streak artifact, and respiratory motion/pulsation artifact (Fig. 2).

To determine the performance of these three protocols without breath-holding in patients who cannot hold their breath for the conventional breath-hold HBP acquisition, one radiologist (S.I.) was also asked to assess respiratory motion artifacts on the Cartesian breath-hold LAVA images to select 'poor breath-hold cases.' We determined 'poor breath-hold cases' as patients with a respiratory motion artifact score of 1–3 on the Cartesian breath-hold LAVA images.

The signal intensity (SI) of the liver, spleen, portal vein (PV), and HCC (if presented) was measured from images with each data set. SI ratios of the liver to spleen ($SIR_{liver/spleen}$), liver to HCC ($SIR_{liver/lesion}$), and liver to PV ($SIR_{liver/PV}$) were calculated as follows:

$$SIR_{liver/spleen} = \frac{SI_{liver}}{SI_{spleen}}$$

$$SIR_{liver/lesion} = \frac{SI_{liver}}{SI_{lesion}}$$

$$SIR_{liver/PV} = \frac{SI_{liver}}{SI_{PV}}$$

Here, SI_{liver}, SI_{spleen}, SI_{lesion}, and SI_{PV} are the SI values for the liver, spleen, HCC, and PV respectively. SIR was measured to identify any difference in image contrast due to the different *k*-space ordering. For quantitative analysis, the largest possible regions of interest were placed on the liver, spleen, HCC, and PV. During the regions of interest placement, large vessels or artifacts were avoided.

In addition, one MR scientist (D.T., with 3 years of experience for MRI application development) who was blinded to the clinical data, performed quantitative analysis of image sharpness by comparing the full width at half maximum (FWHM) of the line spread function (LSF)[17] for the hepatic vein with MATLAB software (version 9.0; Mathworks, Inc., Natick, MA, USA). The LSF derived from the edge response roughly characterizes the spatial resolution of the images, although many factors affect the image quality, such as motion artifacts, partial volume effects, and thermal noise. The edge response was obtained by fitting the one-dimensional profile measured across the liver to the hepatic vein with the error function expressed as follows.

$$\mathrm{ERF}(x') = \frac{2}{\sqrt{\pi}} \int_0^{x'} e^{-t^2}\, dt$$

$$x' = \frac{x - x_0}{\sigma}$$

Here, x is the spatial position of the profile, x_0 is the edge position, and σ denotes the standard deviation for the error function. Then, the LSF can be defined as the deviation of the error function.

$$\mathrm{LSF} = \frac{d}{dx}\mathrm{ERF}(x') = \frac{2}{\sqrt{\pi}} e^{-x^2}$$

Finally, FWHM can be calculated as follows.

$$\mathrm{FWHM} \approx 2\sqrt{2\ln 2\sigma}$$

The profiles with a length of 20 px were extracted manually from the acquired images. The SI of the profiles was normalized to the range [−1, 1]. The fitting was implemented using the non-linear least-squares method to determine the parameters x_0 and σ. The squared norm of the residual less than 0.1 was considered as the convergence criterion because the LSF approach is sensitive to signal-to-noise ratios of the profiles. The profiles that did not meet the criteria were excluded for the analysis. The range for σ was limited from 0 to 25 px to prevent divergence of the parameters.

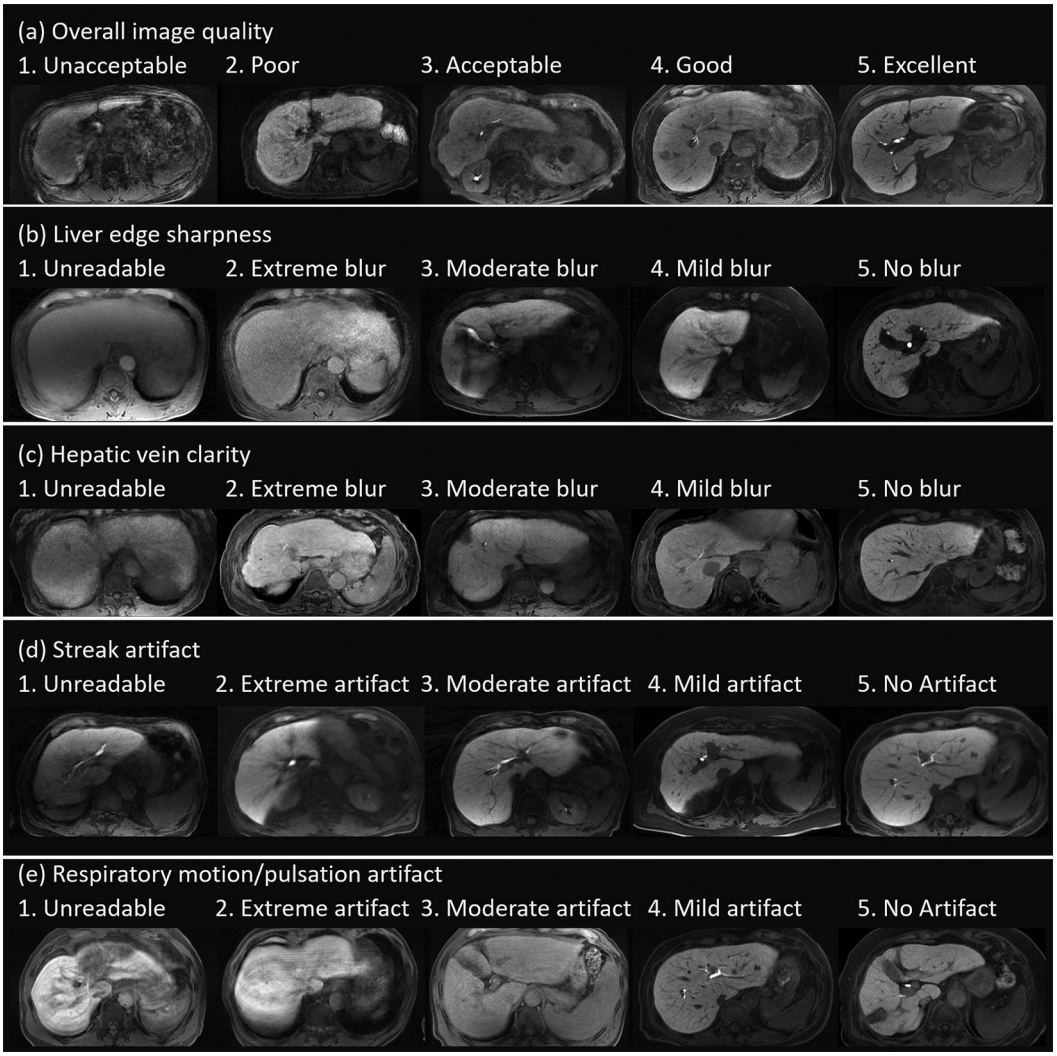

Fig. 2 Examples of images with visual assessment. The following parameters were assessed using a five-point visual score; (**a**) overall image quality (1, unacceptable; 2, poor; 3, acceptable; 4, good; 5, excellent), (**b**) liver edge sharpness (1, unreadable; 2, extreme blur; 3, moderate blur; 4, mild blur; 5, no blur), (**c**) hepatic vein clarity (1, unreadable; 2, extreme blur; 3, moderate blur; 4, mild blur; 5, no blur), (**d**) streak artifact (1, unreadable; 2, extreme artifact; 3, moderate artifact; 4, mild artifact; 5, no artifact), and (**e**) respiratory motion/pulsation artifact (1, unreadable; 2, extreme artifact; 3, moderate artifact; 4, mild artifact; 5, no artifact).

Statistical analysis

The visual assessment findings, $SIR_{liver/spleen}$, $SIR_{liver/lesion}$, $SIR_{liver/PV}$, and FWHM were compared between the three sequences using the Friedman test. Weighted kappa values or intraclass correlation coefficients (ICCs) were calculated to assess inter-observer agreement. Agreement was considered excellent for kappa values (κ) or ICC values (r) > 0.8, good for $0.6 < \kappa$ or $r \leq 0.8$, moderate for $0.4 < \kappa$ or $r \leq 0.6$, fair for $0.2 < \kappa$ or $r \leq 0.4$, and poor for κ or $r \leq 0.2$. All statistical analyses were performed using JMP software (version 12.2.0; SAS Institute Inc., Cary, NC, USA). P-values <0.05 were considered statistically significant.

Results

Image quality between the three sequences

The image quality in LAVA $Star_{navi+}$ (mean score, 4.56 ± 0.66) was better than that in Cartesian $LAVA_{navi+}$ (3.88 ± 0.76) and LAVA $Star_{navi-}$ (3.56 ± 0.68) (both $P < 0.0001$). Cartesian $LAVA_{navi+}$ also showed better image quality than LAVA $Star_{navi-}$ ($P = 0.0106$) (Figs. 3a and 4). Based on the results of blind reading of breath-hold Cartesian LAVA sequences, nine cases were categorized as poor breath-hold cases. Among the poor breath-hold cases, LAVA $Star_{navi+}$ (4.00 ± 0.94) showed better image quality than LAVA $Star_{navi-}$ (2.88 ± 0.74) ($P = 0.0084$). No significant difference was observed between any of the other pairs (Cartesian $LAVA_{navi+}$ [3.22 ± 0.97], $P > 0.0971$) (Figs. 3b and 5).

The score for liver edge sharpness in LAVA $Star_{navi+}$ (4.86 ± 0.35) was higher than that in LAVA $Star_{navi-}$ (4.36 ± 0.96) ($P < 0.0001$). Cartesian $LAVA_{navi+}$ (4.68 ± 0.66) also showed higher scores for liver edge sharpness than LAVA $Star_{navi-}$ ($P = 0.0030$). There was no significant difference in scores for liver edge sharpness between LAVA $Star_{navi+}$ and Cartesian $LAVA_{navi+}$ ($P = 0.1472$) (Fig. 3c).

The score for hepatic vein clarity in LAVA $Star_{navi+}$ (4.61 ± 0.78) was better than that in Cartesian $LAVA_{navi+}$ (3.97 ± 1.18) and LAVA $Star_{navi-}$ (3.71 ± 1.10) (both $P < 0.0001$). Cartesian $LAVA_{navi+}$ also showed higher scores for hepatic vein clarity than LAVA $Star_{navi-}$ ($P = 0.0074$). (Fig. 3d).

In the quantitative assessment for sharpness of images, 27 patients were excluded from the analysis because they did

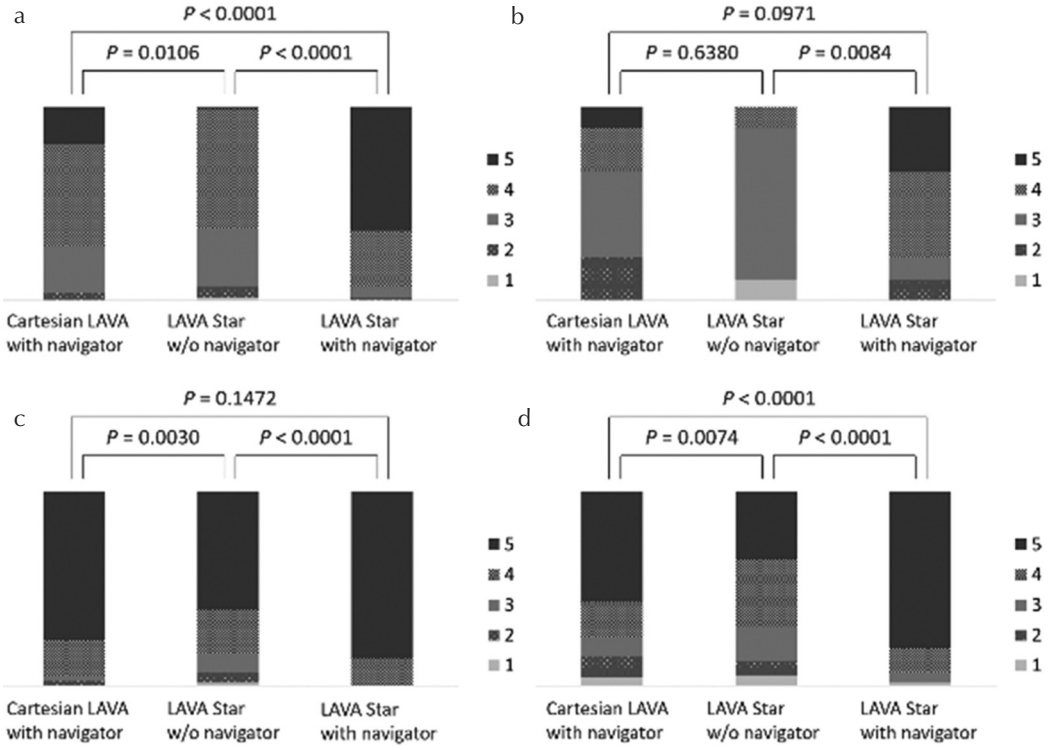

Fig. 3 Stacked bar graph representing results of the visual assessment for the parameters of image quality. (**a**) Overall image quality (all cases), (**b**) overall image quality (poor breath-hold cases [n = 9]), (**c**) liver edge sharpness, (**d**) hepatic vein clarity. (**a**) The image quality of LAVA Star$_{navi+}$ was better than that of Cartesian LAVA$_{navi+}$ and LAVA Star$_{navi-}$. Cartesian LAVA$_{navi+}$ also showed better image quality than LAVA Star$_{navi-}$. (**b**) Among the cases with poor breath-holding, LAVA Star$_{navi+}$ showed better image quality than LAVA Star$_{navi-}$. There were no significant differences observed between Cartesian LAVA$_{navi+}$ and LAVA Star$_{navi-}$ or LAVA Star$_{navi+}$. (**c**) The score for liver edge sharpness of LAVA Star$_{navi+}$ was better than that of Cartesian LAVA$_{navi+}$. Cartesian LAVA$_{navi+}$ also showed a higher score for liver edge sharpness than LAVA Star$_{navi-}$. No significant difference was observed between scores in LAVA Star$_{navi+}$ and Cartesian LAVA$_{navi+}$. (**d**) The score for hepatic vein clarity of LAVA Star$_{navi+}$ was better than that of Cartesian LAVA$_{navi+}$ and LAVA Star$_{navi-}$. Cartesian LAVA$_{navi+}$ also showed higher scores than LAVA Star$_{navi-}$. LAVA, liver acquisition with volume acceleration; LAVA Star$_{navi-}$: stack-of-stars LAVA without navigator echoes; LAVA Star$_{navi+}$: stack-of-stars LAVA with navigator echoes.

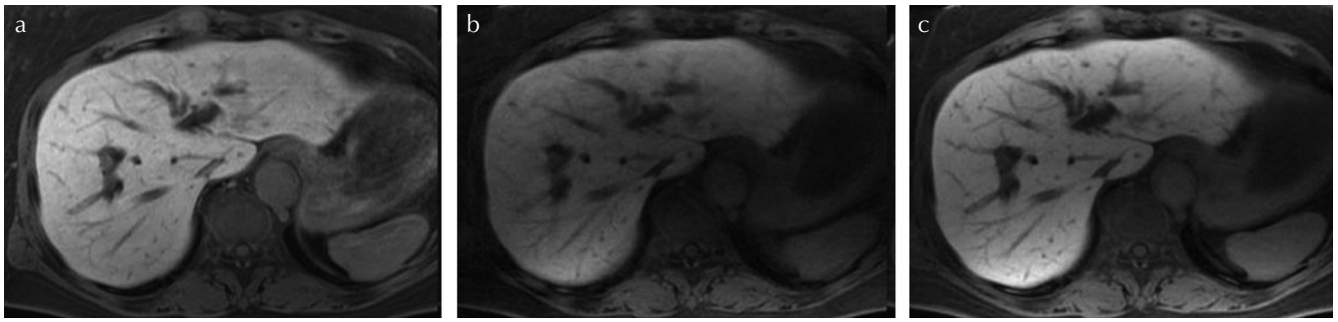

Fig. 4 Comparison of images of the three sequences (good breath-hold case). (**a**) Cartesian liver acquisition with volume acceleration with navigator echoes (Cartesian LAVA$_{navi+}$), (**b**) stack-of-stars LAVA without navigator echoes (LAVA Star$_{navi-}$), and (**c**) stack-of-stars LAVA with navigator echoes (LAVA Star$_{navi+}$). These are the images of a 62-year-old woman with good breath-hold. In this case, Cartesian LAVA$_{navi+}$ and LAVA Star$_{navi+}$ showed similar image quality. The image quality of LAVA Star$_{navi-}$ was lower than that of others; however, severe artifacts were not observed.

not meet the inclusion criteria; therefore, 45 patients were analyzed. LAVA Star$_{navi-}$ (4.80 ± 1.70) showed higher FWHM than Cartesian LAVA$_{navi+}$ (3.77 ± 0.75) and LAVA Star$_{navi+}$ (3.73 ± 0.83) (P = 0.0066 and 0.0031, respectively). There was no significant difference between the FWHM of Cartesian LAVA$_{navi+}$ and LAVA Star$_{navi+}$ (P = 0.9733) (Fig. 6).

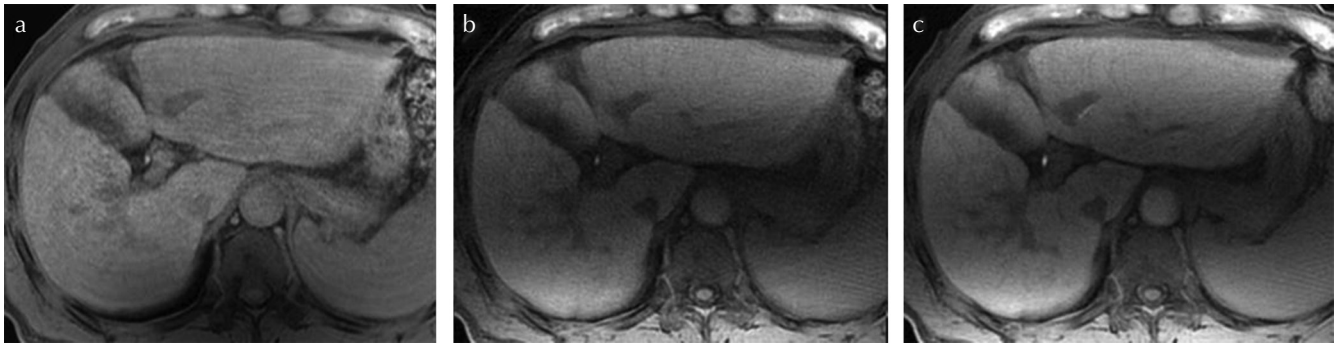

Fig. 5 Comparison of images of the three sequences (poor breath-hold case). (**a**) Cartesian liver acquisition with volume acceleration with navigator echoes (Cartesian $LAVA_{navi+}$), (**b**) stack-of-stars LAVA without navigator echoes (LAVA $Star_{navi-}$), and (**c**) stack-of-stars LAVA with navigator echoes (LAVA $Star_{navi+}$). These are the images of a 65-year-old man with poor breath-hold. In this case, the Cartesian $LAVA_{navi+}$ image showed respiratory motion artifact; however, motion artifacts were not observed in the LAVA Star sequences regardless of the use of navigator echoes. The image quality of LAVA $Star_{navi+}$ was the best in this case. It is assumed that LAVA Star sequence is less likely to be affected by respiratory motion.

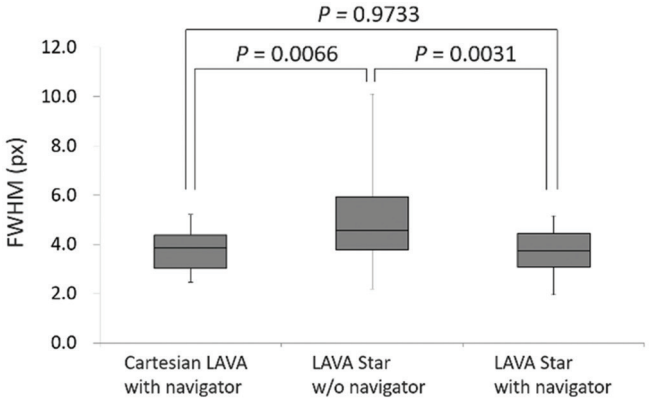

Fig. 6 Box plots representing the FWHM of the line spread function for hepatic vein. LAVA $Star_{navi-}$ showed higher FWHM (= higher blurring) than Cartesian $LAVA_{navi+}$ and LAVA $Star_{navi+}$. There was no significant difference between the FWHM of Cartesian $LAVA_{navi+}$ and that of LAVA $Star_{navi+}$. LAVA, liver acquisition with volume acceleration; LAVA $Star_{navi-}$: stack-of-stars LAVA without navigator echoes; LAVA $Star_{navi+}$: stack-of-stars LAVA with navigator echoes; FWHM, full width at half maximum.

Artifacts between the three sequences

Streak artifacts were observed only on the images of LAVA Star sequences. The LAVA $Star_{navi+}$ images (4.53 ± 0.55) showed fewer streak artifacts than the LAVA $Star_{navi-}$ images (3.51 ± 0.85) ($P < 0.0001$, Fig. 7a). The Cartesian $LAVA_{navi+}$ images (3.93 ± 0.92) had stronger respiratory motion/pulsation artifacts than LAVA $Star_{navi-}$ (4.90 ± 0.30) and LAVA $Star_{navi+}$ (4.89 ± 0.31) images (both $P < 0.0001$). There was no significant difference between the respiratory motion/pulsation artifact scores for LAVA $Star_{navi-}$ and LAVA $Star_{navi+}$ ($P = 1.0000$) (Fig. 7b).

SI ratios between liver and spleen, HCC, and PV

The $SIR_{liver/spleen}$ of LAVA $Star_{navi-}$ (2.12 ± 0.72) was higher than that of Cartesian $LAVA_{navi+}$ (1.71 ± 0.33) and LAVA $Star_{navi+}$ (1.77 ± 0.59) ($P = 0.0005$ and <0.0001, respectively). There was no significant difference between the $SIR_{liver/spleen}$ of Cartesian $LAVA_{navi+}$ and LAVA $Star_{navi+}$ ($P = 0.1228$) (Fig. 8a).

The $SIR_{liver/lesion}$ of Cartesian $LAVA_{navi+}$ (1.49 ± 0.34) was lower than that of LAVA $Star_{navi-}$ (2.06 ± 0.65) and LAVA $Star_{navi+}$ (2.09 ± 0.72) ($P = 0.0108$ and 0.0019, respectively). There was no significant difference between the $SIR_{liver/lesion}$ of LAVA $Star_{navi-}$ and that of LAVA $Star_{navi+}$ ($P = 0.8590$) (Fig. 8b).

The $SIR_{liver/PV}$ of Cartesian $LAVA_{navi+}$ (1.51 ± 0.32) was also lower than that of LAVA $Star_{navi-}$ (2.79 ± 0.86) and LAVA $Star_{navi+}$ (2.70 ± 0.87) (both $P < 0.0001$). There was no significant difference between the $SIR_{liver/PV}$ of LAVA $Star_{navi-}$ and that of LAVA $Star_{navi+}$ ($P = 0.5768$) (Fig. 8c).

Inter-observer agreement

The weighted kappa coefficients of all visual assessments were good to excellent for all sequences ($\kappa = 0.660$–0.873). The interobserver agreements for the measurement of the SIRs were also good to excellent for all sequences ($r = 0.630$–0.875) (Table 2).

Discussion

This retrospective study compared the quality of HBP imaging using the prototype pulse sequences LAVA Star with or without navigator echoes and Cartesian LAVA with navigator echoes. Our results revealed that a combination of stack-of-stars acquisition and navigator echoes (LAVA $Star_{navi+}$) was better than stack-of-stars acquisition without navigator echoes (LAVA $Star_{navi-}$) or Cartesian acquisition with navigator echoes ($LAVA_{navi+}$). LAVA $Star_{navi-}$ showed lower image quality than $LAVA_{navi+}$, indicating that stack-of-stars acquisition itself cannot suppress the respiratory motion artifacts as navigator echoes. Therefore, both stack-of-stars acquisition and navigator echoes may be needed for obtaining high-quality HBP images without breath-holding.

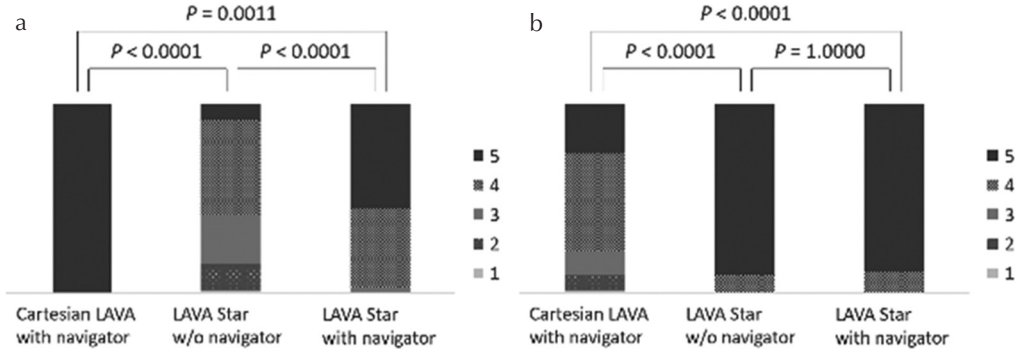

Fig. 7 Stacked bar graph representing the results of the visual assessment for the parameters of artifacts. (**a**) streak artifact, (**b**) respiratory motion/pulsation artifact. (**a**) The images of LAVA $Star_{navi+}$ had less streak artifacts than those of LAVA $Star_{navi-}$, while no streak artifact in Cartesian $LAVA_{navi+}$. (**b**) The images of Cartesian $LAVA_{navi+}$ had stronger respiratory motion/pulsation artifact than those of LAVA $Star_{navi-}$ and LAVA $Star_{navi+}$. There was no significant difference between the score for respiratory motion/pulsation artifact of LAVA $Star_{navi-}$ and that of LAVA $Star_{navi+}$. LAVA, liver acquisition with volume acceleration; LAVA $Star_{navi-}$: stack-of-stars LAVA without navigator echoes; LAVA $Star_{navi+}$: stack-of-stars LAVA with navigator echoes.

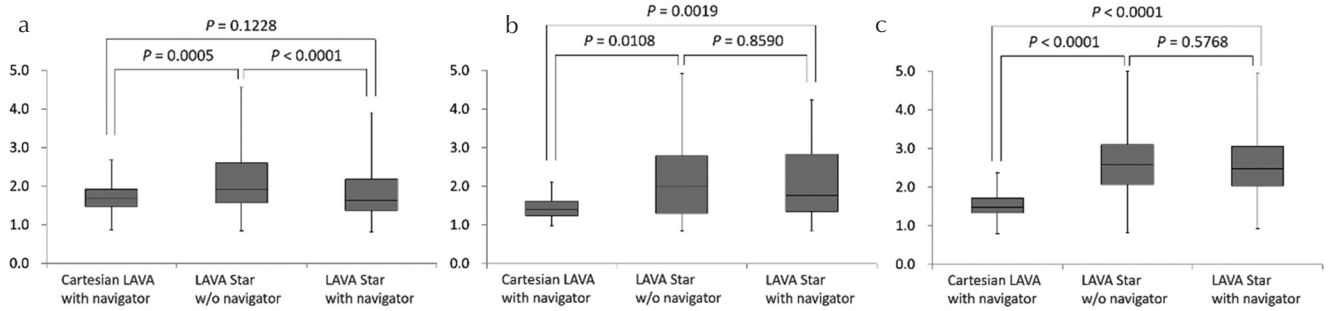

Fig. 8 Box plots of the $SIR_{liver/spleen}$ (**a**) $SIR_{liver/lesion}$ (**b**), and $SIR_{liver/PV}$ (**c**). (**a**) The $SIR_{liver/spleen}$ of LAVA $Star_{navi-}$ was higher than that of Cartesian $LAVA_{navi+}$ and LAVA $Star_{navi+}$. There was no significant difference between the $SIR_{liver/spleen}$ of Cartesian $LAVA_{navi+}$ and that of LAVA $Star_{navi+}$. (**b**) The $SIR_{liver/lesion}$ of Cartesian $LAVA_{navi+}$ was lower than that of LAVA $Star_{navi-}$ and LAVA $Star_{navi+}$. There was no significant difference between the $SIR_{liver/lesion}$ of LAVA $Star_{navi-}$ and that of LAVA $Star_{navi+}$. (**c**) The $SIR_{liver/PV}$ of Cartesian $LAVA_{navi+}$ was also lower than that of LAVA $Star_{navi-}$ and LAVA $Star_{navi+}$. There was no significant difference between the $SIR_{liver/PV}$ of LAVA $Star_{navi-}$ and that of LAVA $Star_{navi+}$. LAVA, liver acquisition with volume acceleration; LAVA $Star_{navi-}$: stack-of-stars LAVA without navigator echoes; LAVA $Star_{navi+}$: stack-of-stars LAVA with navigator echoes; $SIR_{liver/spleen}$, the signal intensity ratios of liver-to-spleen; $SIR_{liver/lesion}$, the signal intensity ratios of liver-to-lesion; $SIR_{liver/PV}$, the signal intensity ratios of liver-to-portal vein

Table 2 Inter-observer agreement of image quality parameter scores and quantitative analysis between two readers

	Cartesian LAVA with navigator echoes	LAVA Star without navigator echoes	LAVA Star with navigator echoes
Overall image quality	0.754 (0.621–0.888)	0.770 (0.634–0.907)	0.759 (0.608–0.909)
Liver edge sharpness	0.660 (0.480–0.840)	0.667 (0.522–0.811)	0.702 (0.480–0.923)
Hepatic vein clarity	0.692 (0.556–0.827)	0.713 (0.585–0.842)	0.745 (0.577–0.913)
Streak artifact	-	0.742 (0.610–0.873)	0.737 (0.586–0.888)
Respiratory motion/pulsation artifact	0.735 (0.597–0.872)	0.860 (0.670–1.000)	0.873 (0.701–1.000)
Signal intensity ratio of liver-to-spleen	0.875 (0.776–0.932)	0.812 (0.671–0.896)	0.805 (0.659–0.892)
Signal intensity ratio of liver-to-lesion	0.756 (0.551–0.875)	0.699 (0.460–0.844)	0.734 (0.515–0.863)
Signal intensity ratio of liver-to-PV	0.643 (0.485–0.760)	0.636 (0.476–0.755)	0.630 (0.469–0.751)

Data are presented as medians and ranges (kappa coefficients for categorical variables and intraclass correlation coefficients for continuous variables). LAVA, liver acquisition with volume acceleration; PV, portal vein.

Although stack-of-stars acquisition is a promising technique, there are still some challenges associated with its use. The acquisition time of LAVA Star$_{navi+}$ was relatively longer than those of the other two protocols. In our study, the scan parameters had the same number of the phase-encoding steps or spokes for each sequence. The reduction in the number of spokes or the use of auto-calibrating reconstruction for Cartesian sampling parallel imaging in the k_z direction can be expected to reduce the scan time in LAVA Star. In our results, the image quality of LAVA Star$_{navi–}$ was not satisfactory high, probably due to respiratory motion that cannot be controlled by simple averaging. One potential solution for this issue involves the use of a soft-gating technique, in which respiratory motion can be controlled by using partial *k*-space data as a monitor for respiratory motion in post-processing.[18] Streak artifacts were another disadvantage of LAVA Star, which was not observed with Cartesian LAVA acquisitions. The images of LAVA Star$_{navi–}$ had more streak artifacts than those of LAVA Star$_{navi+}$. It is interesting to note that streak artifacts were negligible when the acquisition was combined with navigator echoes. It has been reported that the streak artifact can be enhanced by the reduction of the number of radial spokes.[19] Also, in computed tomography, patient motion can cause misregistration of artifacts, which usually appear as shading or streaking on the reconstructed image.[20] In this study, the same number of radial spokes was used in LAVA Star$_{navi+}$ and LAVA Star$_{navi–}$ acquisitions, therefore, the more streak artifact in LAVA Star$_{navi–}$ compared with LAVA Star$_{navi+}$ would be attributed from the respiratory motion. Our results indicate that navigator echoes significantly reduce the motion-induced streak artifacts.

In HBP images obtained using a 3T scanner, image non-uniformity may influence visual and quantitative evaluations. Phased-array uniformity enhancement, a calibration-based method for non-uniformity correction, has been reported as one of the solutions for this problem,[21] and it may be possible to further improve the quality of HBP images by combining this method with LAVA Star.

In this study, image quality and hepatic vein clarity score in LAVA Star$_{navi+}$ was better than that in Cartesian LAVA$_{navi+}$. There may be two explanations for this. First, the respiratory motion/pulsation artifacts, which can be observed in the phase encoding direction in Cartesian acquisition. The LAVA Star$_{navi+}$ images had fewer respiratory motion/pulsation artifacts than Cartesian LAVA$_{navi+}$. Second, the sampling differences. LAVA Star acquisition uses 320-points radial sampling in the $k_x - k_y$ plane, which results in isotropic in-plane spatial resolution. In contrast, conventional Cartesian acquisition involves partial Fourier acquisition with parallel imaging in the k_y direction. Therefore, LAVA Star has more spatial information than conventional Cartesian acquisition, which would result in improved overall image quality score in LAVA Star$_{navi+}$ compared with Cartesian LAVA$_{navi+}$.

In our results, the SIR$_{liver/spleen}$ of LAVA Star$_{navi–}$ was higher than that of Cartesian LAVA$_{navi+}$ and LAVA Star$_{navi+}$. This result suggested that the T_1 contrast can be decreased by navigator echoes. In the navigator technique, the longitudinal magnetization recovers during the waiting time of navigator triggering. This reduces the T_1 contrast and increases the SI of the objects.[22] In addition, the SIR$_{liver/lesion}$ and SIR$_{liver/PV}$ of Cartesian LAVA$_{navi+}$ were lower than those of LAVA Star$_{navi–}$ and LAVA Star$_{navi+}$. Delay after injection with Cartesian LAVA$_{navi+}$ was 15 min in this study. The other sequences were started 18–23 min after injection. The SI of the liver increases up to approximately 20 min after injection[1]; therefore, the difference in delay time among the three sequences might influence the SIR$_{liver/lesion}$ and SIR$_{liver/PV}$ results.

Limitations

Our study has some limitations. First, we did not evaluate the diagnostic performance of focal hepatic lesions, although we believe that LAVA Star$_{navi+}$ could show a high diagnostic performance because of its excellent image quality. Second, the three sequences were obtained in a fixed order. We could not exclude the influence of delay time on the image contrast, because the liver enhancement might differ during the hepatobiliary phase. Further studies are expected to address the image contrast of stack-of-stars acquisition in pre- and post-contrast imaging. Third, there was small number of poor breath-hold cases. From a clinical perspective, it is most important to determine whether stack-of-stars acquisition is useful for poor breath-hold cases. Among the poor breath-hold cases, no significant difference was observed between overall image quality between LAVA Star$_{navi+}$ and Cartesian LAVA$_{navi+}$; however, these differences were marginally significant ($P = 0.0971$). Further studies that evaluate the image quality of stack-of-stars acquisition in poor breath-hold cases are required.

Conclusion

The use of both stack-of-stars acquisition and navigator echoes is the best solution to obtain HBP images without breath-holding in terms of the quality of images.

Conflicts of Interest

We acknowledge a financial support from GE Healthcare on this project. Co-authors, Tetsuya Wakayama, Kang Wang, Ty A Cashen, and Ali Ersoz are employees of GE Healthcare. The remaining authors have no other conflicts of interest related to this submission personally.

References

1. Hamm B, Staks T, Mühler A, et al. Phase I clinical evaluation of Gd-EOB-DTPA as a hepatobiliary MR contrast agent: safety, pharmacokinetics, and MR imaging. Radiology 1995; 195:785–792.

2. Joo I, Lee JM, Lee DH, Jeon JH, Han JK. Retrospective validation of a new diagnostic criterion for hepatocellular carcinoma on gadoxetic acid-enhanced MRI: can hypointensity on the hepatobiliary phase be used as an alternative to washout with the aid of ancillary features? Eur Radiol 2019; 29: 1724–1732.
3. Yoon JH, Lee JM, Lee YJ, Lee KB, Han JK. Added value of sequentially performed gadoxetic acid-enhanced liver MRI for the diagnosis of small (10-19 mm) or atypical hepatic observations at contrast-enhanced CT: a prospective comparison. J Magn Reson Imaging 2019; 49:574–587.
4. Asato N, Tsurusaki M, Sofue K, et al. Comparison of gadoxetic acid-enhanced dynamic MR imaging and contrast-enhanced computed tomography for preoperative evaluation of colorectal liver metastases. Jpn J Radiol 2017; 35:197–205.
5. Ogasawara G, Inoue Y, Matsunaga K, et al. Evaluation of a respiratory navigator-gating technique in Gd-EOB-DTPA-enhanced magnetic resonance imaging for the assessment of liver tumors. Eur J Radiol 2016; 85:1232–1237.
6. Yoon JH, Lee JM, Lee ES, et al. Navigated three-dimensional T_1-weighted gradient-echo sequence for gadoxetic acid liver magnetic resonance imaging in patients with limited breath-holding capacity. Abdom Imaging 2015; 40:278–288.
7. Peters DC, Korosec FR, Grist TM, et al. Undersampled projection reconstruction applied to MR angiography. Magn Reson Med 2000; 43:91–101.
8. Budjan J, Riffel P, Ong MM, Schoenberg SO, Attenberger UI, Hausmann D. Rapid Cartesian versus radial acquisition: comparison of two sequences for hepatobiliary phase MRI at 3 tesla in patients with impaired breath-hold capabilities. BMC Med Imaging 2017; 17:32.
9. Kurozumi M, Fujinaga Y, Kitou Y, et al. Evaluation of hemodynamic imaging findings of hypervascular hepatocellular carcinoma: comparison between dynamic contrast-enhanced magnetic resonance imaging using radial volumetric imaging breath-hold examination with k-space-weighted image contrast reconstruction and dynamic computed tomography during hepatic arteriography. Jpn J Radiol 2018; 36:295–302.
10. Glover GH, Pauly JM. Projection reconstruction techniques for reduction of motion effects in MRI. Magn Reson Med 1992; 28:275–289.
11. Peters DC, Derbyshire JA, McVeigh ER. Centering the projection reconstruction trajectory: reducing gradient delay errors. Magn Reson Med 2003; 50:1–6.
12. Kajita K, Goshima S, Noda Y, et al. Thin-slice free-breathing pseudo-golden-angle radial stack-of-stars with gating and tracking T_1-weighted acquisition: an efficient gadoxetic acid-enhanced hepatobiliary-phase imaging alternative for patients with unstable breath holding. Magn Reson Med Sci 2019; 18:4–11.
13. Chandarana H, Block TK, Rosenkrantz AB, et al. Free-breathing radial 3D fat-suppressed T1-weighted gradient echo sequence: a viable alternative for contrast-enhanced liver imaging in patients unable to suspend respiration. Invest Radiol 2011; 46:648–653.
14. Weiss J, Taron J, Othman AE, et al. Feasibility of self-gated isotropic radial late-phase MR imaging of the liver. Eur Radiol 2017; 27:985–994.
15. Jackson JI, Meyer CH, Nishimura DG, Macovski A. Selection of a convolution function for Fourier inversion using gridding [computerised tomography application]. IEEE Trans Med Imaging 1991; 10:473–478.
16. Beatty PJ, Nishimura DG, Pauly JM. Rapid gridding reconstruction with a minimal oversampling ratio. IEEE Trans Med Imaging 2005; 24:799–808.
17. McRobbie DW. A three-dimensional volumetric test object for geometry evaluation in magnetic resonance imaging. Med Phys 1997; 24:737–742.
18. Johnson KM, Block WF, Reeder SB, Samsonov A. Improved least squares MR image reconstruction using estimates of *k*-space data consistency. Magn Reson Med 2012; 67:1600–1608.
19. Xue Y, Yu J, Kang HS, Englander S, Rosen MA, Song HK. Automatic coil selection for streak artifact reduction in radial MRI. Magn Reson Med 2012; 67:470–476.
20. Barrett JF, Keat N. Artifacts in CT: recognition and avoidance. Radiographics 2004; 24:1679–1691.
21. Ogasawara G, Inoue Y, Matsunaga K, Fujii K, Hata H, Takato Y. Image non-uniformity correction for 3T Gd-EOB-DTPA-enhanced MR imaging of the liver. Magn Reson Med Sci 2017; 16:115–122.
22. Fujiwara Y, Maruyama H, Kosaka N, Ishimori Y. Simultaneous acquisition of high-contrast and quantitative liver T_1 images using 3D phase-sensitive inversion recovery: a feasibility study. Acta Radiol 2017; 58:899–905.